

Effect of targeted dropsonde observations and best track data on the track forecasts of Typhoon Sinlaku (2008) using an ensemble Kalman filter

By BYOUNG-JOO JUNG¹, HYUN MEE KIM^{1*}, FUQING ZHANG² AND CHUN-CHIEH WU³, ¹*Atmospheric Predictability and Data Assimilation Laboratory, Department of Atmospheric Sciences, Yonsei University, Shinchon-dong 134, Seodaemun-gu, Seoul, 120-749, Republic of Korea;* ²*Department of Meteorology, Pennsylvania State University, Pennsylvania, PA, USA;* ³*Department of Atmospheric Sciences, National Taiwan University, Taipei, Taiwan*

(Manuscript received 13 June 2011; in final form 10 October 2011)

ABSTRACT

During August and September 2008, The Observing System Research and Predictability Experiment (THORPEX) – Pacific Asian Regional Campaign (T-PARC) was conducted to investigate the formation, structure, targeted observation, extratropical transition (ET) and downstream effects of tropical cyclones (TCs) in the Western North Pacific (WNP) region. This study investigates the effect of targeted dropsonde observations from T-PARC and the TC best track data on the track forecast of Typhoon Sinlaku (2008). A WRF-based ensemble Kalman filter (EnKF) is used for a series of observation system experiments (OSEs). From the innovation statistics and rank histograms, the EnKF behaves well in terms of ensemble spread, despite some spread deficiency in low-tropospheric winds and warm and moist biases. Assimilation of targeted dropsonde observations leads to improved initial position and subsequent track forecast compared with experiments that only assimilate conventional observations. In the meantime, assimilation of TC position reduces the initial position error, whereas assimilation of minimum sea level pressure (SLP) information is efficient to analyse the strong vortex structures of TC and reduces track forecast errors. Assimilation of TC position and minimum SLP information is particularly beneficial when dropsonde observations do not exist.

Keywords: Ensemble kalman filter, typhoon track forecast, targeted dropsonde observations, typhoon best track data, T-PARC

1. Introduction

Tropical cyclones (TCs) are one of the most destructive phenomena in nature, characterised by strong wind and severe precipitation. Even though the analysis and prediction of TCs are constrained by the sparse observation network over the ocean, there has been a steady increase in predictability because of the improvement of analysis and forecast systems. The increased model resolution and sophisticated sub-grid scale parameterisations from better understandings of dynamics and physical processes contributed to the improvement of forecast systems. The improvement of analysis systems is obtained by the growing use of satellite-derived observations (e.g. Huang

et al., 2005; Velden et al., 2005; Anthes et al., 2008; Pu et al., 2008; Langland et al., 2009) and dropsonde observations (e.g. Burpee et al., 1996; Aberson, 2002, 2010; Wu et al., 2005), as well as through the improvement of analysis systems and initialisation techniques (e.g. Kurihara et al., 1995; Zou and Xiao, 2000; Pu and Braun, 2001; Wu et al., 2006; Xiao et al., 2006, 2008; Chou and Wu, 2008; Hsiao et al., 2010).

Dropsonde observations have been widely utilised for TC surveillance programmes. Since 1982, dropsonde observations were used in the Hurricane Research Division (HRD) of the National Oceanic and Atmospheric Administration (NOAA) to enhance the number of in situ observations in the core and surrounding environment of hurricanes (Burpee et al., 1996). By assimilating dropsonde observations, the TC track error decreased by approximately 16–30%, which is comparable to the accumulated

*Corresponding author.
email: khm@yonsei.ac.kr

improvement during the previous 20–25 yr (Burpee et al., 1996). Since 1997, the synoptic surveillance programme has been operated in the HRD, and dropsonde observations have contributed to the improvement in track forecasting (Aberson and Franklin, 1999; Aberson, 2002, 2010). For the Western North Pacific (WNP) region, the Dropwindsonde Observations for Typhoon Surveillance near the Taiwan Region (DOTSTAR) has been in operation since 2003 (Wu et al., 2005). In 2004, a 22% average improvement in the 72-h track forecast was demonstrated using four operational and one research models for 10 missions of DOTSTAR (Wu et al., 2007).

Due to the limited airborne observations in field programmes, the sensitivity guidance that detects the most important region in the initial field for forecast improvement was developed in the context of adaptive (or targeted) observations (Langland, 2005; Majumdar et al., 2006; Reynolds et al., 2007; Wu et al., 2009; Kim and Jung, 2009a,b). Aberson (2003) reported that the assimilation of only a subset of the data from subjectively sampled target regions produced a statistically significant 25% reduction in track error. Aberson and Etherton (2006) also observed additional improvement in track forecast using the ensemble transform Kalman filter (ETKF; Bishop et al., 2001). Yamaguchi et al. (2009) found that dropsonde observations over sensitive regions indicated by singular vectors (SVs; Palmer et al., 1998; Kim and Morgan, 2002; Peng and Reynolds, 2006; Buizza et al., 2007) were more important than were those over the non-sensitive regions for the forecast of TC Conson (200404) using the Japan Meteorological Agency (JMA) global model and four-dimensional variational (4DVAR) data assimilation system. Aberson et al. (2011) applied three different targeting strategies (ensemble variance, ETKF and SV) to synoptic surveillance cases during 2004–2006 using the National Centre for Environmental Prediction (NCEP) Global Forecast System (GFS) and a three-dimensional variational (3DVAR) assimilation system. Compared with using all available dropsonde observations, the dropsonde sampled via the SV strategy reduced the 24–72 h forecast track error, while the dropsonde sampled using ensemble variance and ETKF reduced the 84 and 108 h forecast track errors, all at an 85% confidence level. These values suggest that the use of targeting strategies is beneficial to identify the amplifying error.

During August and September 2008, The Observing System Research and Predictability Experiment (THORPEX) – Pacific Asian Regional Campaign (T-PARC) was implemented in the WNP region to investigate the formation, structure, targeted observation, extratropical transition (ET) and downstream effects of tropical cyclones (TCs) based on international collaboration (Elsberry and Harr, 2008; Parsons et al., 2008; Rabier et al., 2008).

For T-PARC cases, Weissmann et al. (2011) evaluated the effect of targeted dropsonde observations on track forecasts in the global models of the European Centre for Medium-range Weather Forecasts (ECMWF), the JMA, the NCEP and the regional Korea Meteorological Administration (KMA) Weather Research and Forecasting (WRF) model. The improvements in the JMA and ECMWF models were small compared with the 20–40% improvements in the NCEP and WRF models because the JMA and ECMWF use the more advanced data assimilation system (i.e. 4DVAR) and substantial satellite observations. Also, Harnisch and Weissmann (2010) evaluated the impacts of three different subsets of dropsonde observations (core of TC, vicinity of TC and remote from TC) in the ECMWF model and found that the dropsonde observations in the vicinity of the TC were the most helpful for typhoon (TY) track forecasts. After evaluating 42 surveillance cases from DOTSTAR and T-PARC, Chou et al. (2011) reported that the assimilation of dropsonde observations could lead to improvements in 1- to 5-day track forecasts, as well as a 10–20% mean track error reduction. Similarly, using the WRF model and 3DVAR assimilation system, Jung et al. (2010) noticed positive effects of the targeted dropsonde observations on the track forecast of TC Jangmi (200815), observed during T-PARC.

With the increase in high-performance computing facilities, the EnKF data assimilation system has been extensively employed with global forecast models (Houtekamer et al., 2005; Szunyogh et al., 2008; Whitaker et al., 2008; Hamill et al., 2011), mesoscale systems (Torn et al., 2006; Zhang et al., 2006; Meng and Zhang, 2007, 2008a,b; Torn and Hakim, 2008; Torn, 2010) and convective-scale systems (Snyder and Zhang, 2003; Zhang et al., 2004; Xue and Martin, 2006; Aksoy et al., 2009; refer to Meng and Zhang, 2011 for a complete review on the recent development and applications of the EnKF for limited-area data assimilation). Recently, the EnKF system has also been used for the initialisation and forecast of TCs (Torn and Hakim, 2009; Zhang et al., 2009; Weng et al., 2011). The ensemble data assimilation system can easily assimilate TC information (e.g. location, intensity, motion vectors and axisymmetric surface wind structures) as observations (Chen and Snyder, 2007; Torn, 2010; Wu et al., 2010; Hamill et al., 2011). Nevertheless, the previous T-PARC studies did not use the EnKF data assimilation system to assimilate targeted dropsonde observations and TC track information. Because EnKF is very convenient for the assimilation of TC parameters (e.g. latitude and longitude of TC centre, minimum sea level pressure [SLP]), as well as for general observations of the TC, the effects of the best track information and the targeted dropsonde observations on the TC track forecasts can be evaluated

and compared using EnKF. Thus, in this study, the effects of targeted dropsonde observations as well as position and intensity information of TC tracks on track forecasts are evaluated and compared for TC Sinlaku (2008). The data for this study were collected during T-PARC and were analysed using EnKF with flow-dependent error covariance. In addition, the effect of dropsonde observations over the TC core regions is also evaluated in the same framework. The case description for TC Sinlaku is presented in Section 2. Experimental design and model configurations are given in Section 3. Main results are shown in Section 4, and the summary and discussions are presented in Section 5.

2. Case description of TC Sinlaku (200813)

TC Sinlaku (200813) first developed over the eastern ocean of the Philippines and moved northwestward (Fig. 1a). It progressed to the tropical storm¹ (TS) stage at 1800 UTC 8 September 2008. It then intensified very rapidly and reached the TY stage at 1200 UTC 9 September 2008 (Figs. 1b and 2a). During this rapid development,² the maximum sustained surface winds increased at a rate of 15 m s^{-1} over 18 h ($\sim 20 \text{ m s}^{-1}$ over 24 h). As the WNP high moved to the east, Sinlaku moved to the northeast after 0000 UTC 10 and reached its maximum intensity with a central pressure of 935 hPa and maximum sustained surface winds of 100 kt at 1200 UTC 10 (Figs 1b and 2b). This maximum intensity was maintained for 1 day. After 0000 UTC 12, it moved to the northwest toward Taiwan. From 1200 UTC 12, the WNP high expanded to the west. As it neared Taiwan, Sinlaku started to weaken after 1200 UTC 13 and made landfall near the northeast coast of Taiwan around 1600 UTC 13 September 2008 (Fig. 2c). It subsequently began to recurve and interact with the mid-latitude system and WNP high (Fig. 2d). Sinlaku then moved eastward and passed over the southern ocean of Japan (Fig. 1a) and re-intensified on 19 September 2008 (Fig. 1b). After 21 September, it underwent ET. Observation system experiments (OSEs) using the EnKF data assimilation system were performed from 0000 UTC 9 to 0000 UTC 12 September 2008 (Fig. 1b), when the TC was rapidly developing and was approaching Taiwan. There were intensive, targeted flights during this period.

¹Based on the RSMC Tokyo, the TC scales are categorised as tropical depression (TD), tropical storm (TS), severe tropical storm (STS), and typhoon (TY).

²Kaplan and DeMaria (2003) defined tropical cyclones (TCs) that intensify at a rate of 15 m s^{-1} over 24 h as ‘rapidly intensifying TCs’.

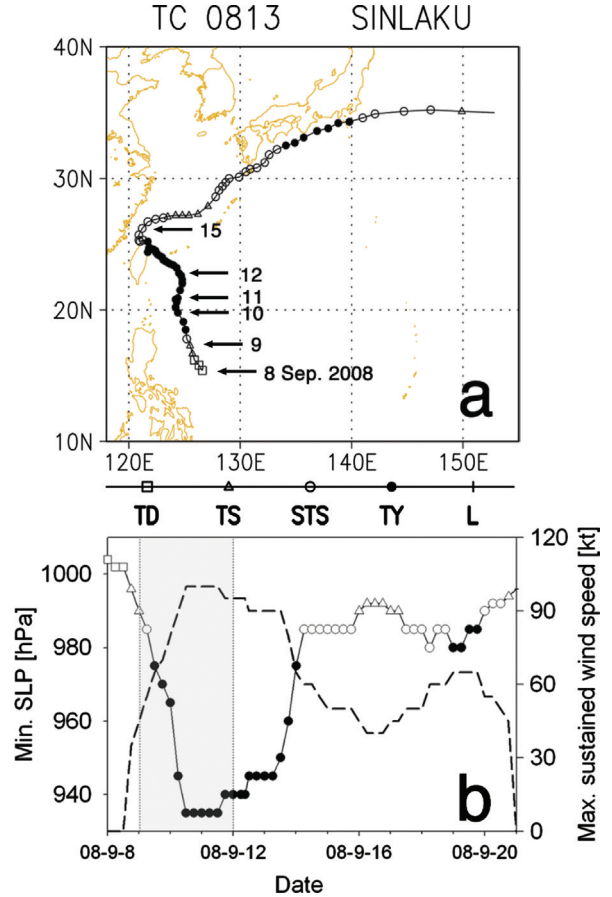


Fig. 1. (a) Best track; and (b) minimum sea level pressure (SLP, hPa) of TC Sinlaku (200813) from the Regional Specialised Meteorological Centre (RSMC) Tokyo. The shaded area in (b) represents the period of time over which the data assimilation was performed.

3. Experimental framework

3.1. Model

For the forecast model, the Advanced Research WRF modeling system version 2.2 (Skamarock et al., 2005) was used. Two nested domains with grid distances of 45 km (domain 1) and 15 km (domain 2) were established with one-way nesting configuration, centred at 25°N , 125°E in the East Asian and WNP regions. The multiple combinations of cumulus (CU), microphysics (MP), and planetary boundary layer (PBL) physics schemes were used for each ensemble member differently in order to consider the model error (Table 1). Three CU schemes [Kain–Fritsch [Kain and Fritsch, 1993; Kain, 2004], Betts–Miller–Janjić [Betts, 1986; Betts and Miller, 1986; Janjić, 1994], and Grell–Devenyi [Grell, 1993; Grell

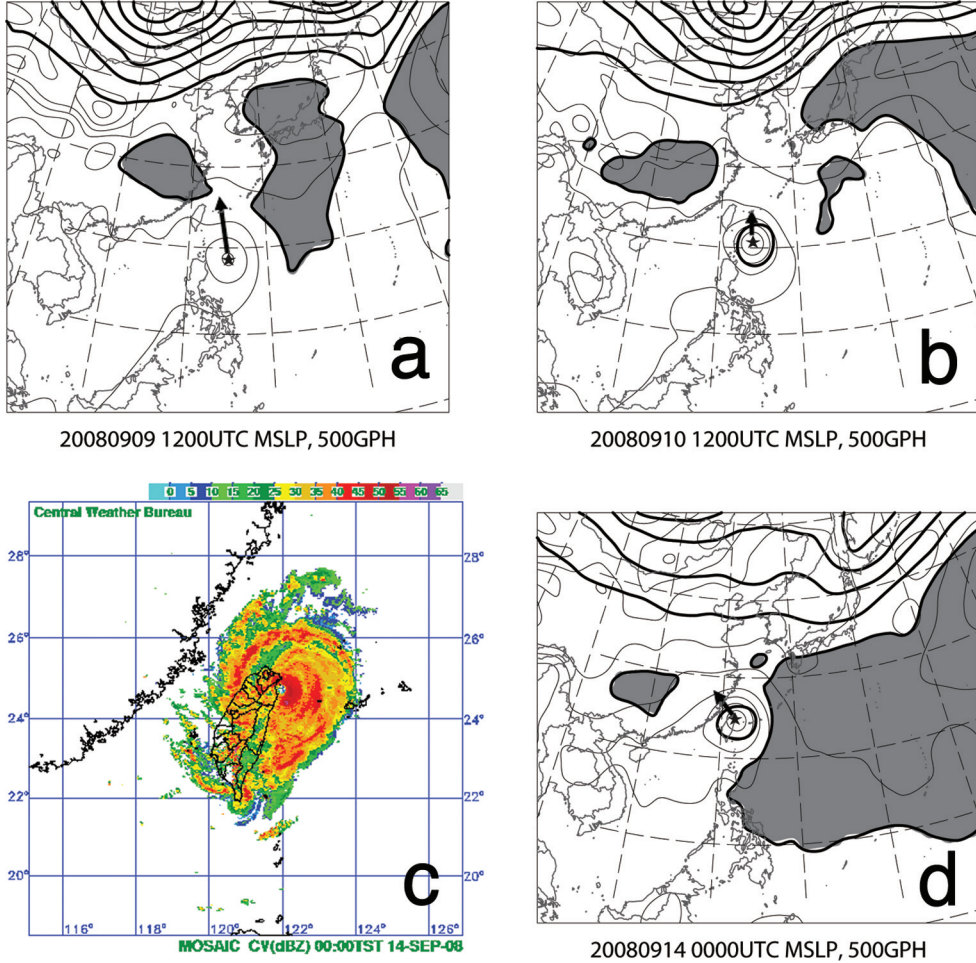


Fig. 2. SLP (thin lines at 4 hPa intervals) and geopotential height (thick lines at intervals of 60 gpm) on 500 hPa of NCEP FNL at: (a) 1200 UTC 9; (b) 1200 UTC 10; and (d) 0000 UTC 14 September 2008. The shaded area denotes the subtropical ridge (over 5880 gpm), and the thick arrows indicate the translational velocity of TC Sinlaku. The radar reflectivity (shaded, at 5 dBZ intervals) from the Central Weather Bureau (CWB) of Taiwan for 1600 UTC 13 September 2008 is shown in (c).

and Devenyi, 2002)], three MP schemes (Lin [Lin et al., 1983], Thompson [Thompson et al., 2004], and WRF single momentum six-class graupel [WSM6; Hong et al., 2004; Hong and Lim, 2006]), and two PBL schemes (Yonsei University [YSU; Noh et al., 2003; Hong et al., 2006] and Mellor–Yamada–Janjic [MYJ; Mellor and Yamada, 1982; Janjić, 2002]) were employed as the multiple physics options. Except for the CU, MP, and PBL physics schemes, same physics parameterisations for other sub-grid scale processes were used for each ensemble member: the Dudhia scheme (Dudhia, 1989) for shortwave radiation parameterisation, the Rapid Radiative Transfer Model (RRTM) scheme (Mlawer et al., 1997) for long-wave radiation parameterisation, and the Noah Land Surface model (Chen and Dudhia, 2001) for land surface parameterisation.

3.2. Ensemble Kalman filter (EnKF)

The WRF-based ensemble Kalman filter (EnKF) data assimilation system developed in Meng and Zhang (2008a,b) is used for the current study, which is a serial, square-root version (Whitaker and Hamill, 2002; Snyder and Zhang, 2003) of the deterministic algorithms of EnKF (Evensen, 1994; Tippett et al., 2003). Observations are serially assimilated under the assumption that the observations are independent of one another. In this study, 36 ensemble members were used. To control the spurious correlation from long-distance grids due to the limited ensemble size (e.g. sampling error; Hamill et al., 2001; Houtekamer and Mitchell, 2001), the covariance localisation technique was applied using the fifth-order function of Gaspari and Cohn (1999) with a 1800-km localisation radius. To avoid filter divergence due to the small

Table 1. Multiple physics configuration for the ensembles

No. of members using the CU scheme and the scheme used	No. of members using the MP scheme and the scheme used	No. of members using the PBL scheme and the scheme used
12, Kain–Fritsch	4, Lin 4, Thompson 4, WSM6	2, YSU; 2, MYJ 2, YSU; 2, MYJ 2, YSU; 2, MYJ
12, Betts–Miller–Janjic	4, Lin 4, Thompson 4, WSM6	2, YSU; 2, MYJ 2, YSU; 2, MYJ 2, YSU; 2, MYJ
12, Grell–Devenyi	4, Lin 4, Thompson 4, WSM6	2, YSU; 2, MYJ 2, YSU; 2, MYJ 2, YSU; 2, MYJ

ensemble spread, a covariance relaxation (Zhang et al., 2004) of 0.8 prior weighting was applied. To include the model uncertainties in the EnKF analysis, the multiple-physics approach as developed in Meng and Zhang (2007, 2008a,b) is used, in which different ensemble members use different physics parameterisation schemes as listed in Table 1.

3.3. Observations

Figure 3 shows the observation distributions at 0000 UTC 10 September 2008. The surface observations were mainly distributed over the land (Fig. 3a). There were ship, buoy, and station observations on the islands over the ocean. Upper-air radiosonde observations were distributed over the land and several islands (Fig. 3b). Aircraft observations³ were distributed following the pathways of commercial aircrafts (Fig. 3c). Due to the continuous observation reports from aircrafts, these observations were filtered so that they were located at least 100 km (horizontally) and 50 hPa (vertically) from one another. The above-surface, upper-air, and aircraft observations were collected from the Global Telecommunication System (GTS) of KMA.⁴ The targeted dropsonde observations were gathered from four aircrafts (the US Air Force WC-130, the Naval Research Laboratory (NRL) P-3, the Deutsches Zentrum Für Luft- und Raumfahrt (DLR) Falcon and Astra from DOTSTAR) operated during T-PARC. The targeted dropsonde observations were circularly distributed near the TC at 0000 UTC 10 September 2008 (Fig. 3b). The atmospheric motion vectors (AMVs) that were retrieved from the

infrared (IR), shortwave infrared (SWIR), and visible (VIS) channels of the Multi-functional Transport Satellite (MTSAT) were from the Cooperative Institute for Meteorological Satellite Studies (CIMSS; Velden et al., 2005). The super-obs (SOs) of the AMVs are constructed by averaging the AMVs in the $1^\circ \times 1^\circ \times 50$ hPa cubic to reduce the correlation of AMVs (Bormann et al., 2003; Torn and Hakim, 2008). The AMV SOs fully covered the model domain, with many of them located in the upper troposphere (Fig. 3d).

Figure 4 shows the distributions of targeted dropsonde observations during the EnKF analysis period of the experiments. During this period, the four aircrafts were mainly operated for the TC structure observations (Fig. 4a, c, d, f) and TC targeted observations (Fig. 4b, d–f). The targeted dropsonde observations over the inner-core region occurred when the WC-130 aircraft was performing the TC structure observations (Fig. 4a, c, f).

3.4. Experiments

Initial ensemble perturbations were constructed by adding random perturbations, based on the NCEP GFS background error statistics (BES), to the NCEP final analysis (FNL) at 1200 UTC 8 September 2008 (Meng and Zhang, 2008a,b; Torn and Hakim, 2008). The perturbations for lateral boundary condition are also made using the same method with the initial ensemble perturbations while the sea surface temperature (SST) perturbations are not considered. After the initial ensembles were integrated for 12 h, the first EnKF analysis began at 0000 UTC 9 September 2008, and EnKF cycling data assimilations were performed with 6-h assimilation intervals until 0000 UTC 12 September 2008. Three-day ensemble forecasts, initiated at 0000 UTC 10, 0000 UTC 11, and 0000 UTC 12 September 2008, were conducted.

A total of six sets of experiments were conducted to investigate the effects of targeted dropsonde observations

³Since data collection was infeasible at the time of the experiments, flight-level observations from the four T-PARC aircrafts were not used in this study.

⁴For the quality control (QC; e.g. gross check and consistency check) of observations, the pre-processes of WRF data assimilation system are used (Skamarock et al., 2005).

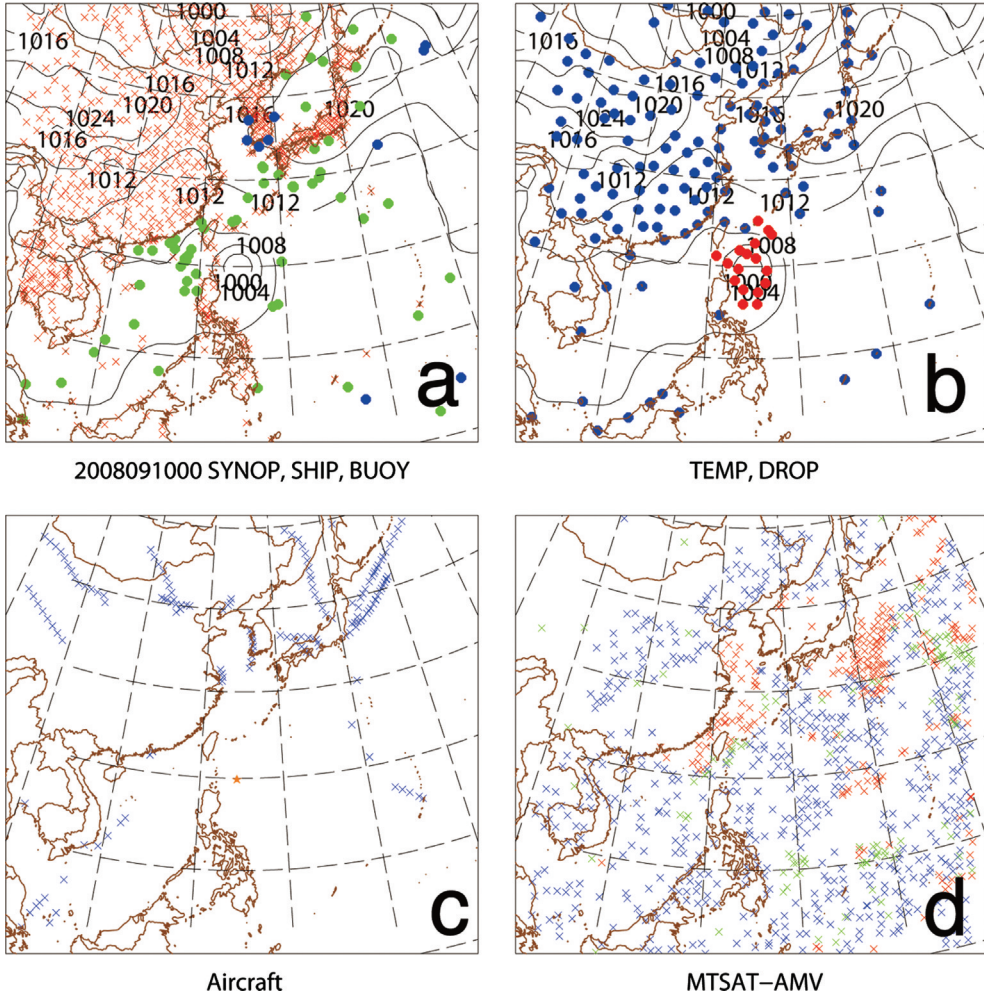


Fig. 3. Observational distribution for: (a) surface observations (red cross for station [SYNOP], blue dot for buoy, and green dot for ship); (b) upper air observations (blue dot for radiosonde and red dot for targeted dropsonde); (c) aircraft observations (blue cross) and position of best track (orange star); and (d) AMV from MTSAT (blue, red, and green for upper-, mid- and lower-troposphere, respectively) at 0000 UTC 10 September 2008. The SLP (solid lines at 4 hPa intervals) of NCEP FNL are superposed on (a) and (b).

and TC best track information on the TC track forecast (Table 2). As a reference experiment, EXP1 assimilated only conventional observations that included surface observations over land and sea, upper-air observations, aircraft observations and the AMVs. EXP2 assimilated conventional observations as well as targeted dropsonde observations from the four aircraft operations to evaluate the effect of the targeted dropsonde observations. EXP3 was designed to evaluate the effect of TC position information. The best track from the Regional Specialised Meteorological Centre (RSMC) Tokyo was used for position and SLP information. The assimilation of position information was conducted similarly to the method of Chen and Snyder (2007). Because the background error covariance is calculated using ensembles, the position of the TC could be assimilated in EnKF. EXP4 assimilated the

conventional observations, TC position, and minimum SLP information. EXP5 assimilated conventional observations, targeted dropsonde observations, and TC position and SLP information to evaluate the combined impact of all observations used in this study.

For EXP2 and EXP5, the targeted dropsonde observations near the TC core regions were not assimilated. Aberson (2008) suggested that the assimilation of dropsonde observations over the inner-core region could degrade the TC forecast due to a lack of representation of inner-core structure in the model fields. Recently, Harnisch and Weissmann (2010) reported a neutral effect of assimilating dropsonde observations near the core regions using the ECMWF system, while Weissmann et al. (2011) reported a negative effect for two cases in the JMA system. To evaluate the effect of dropsondes

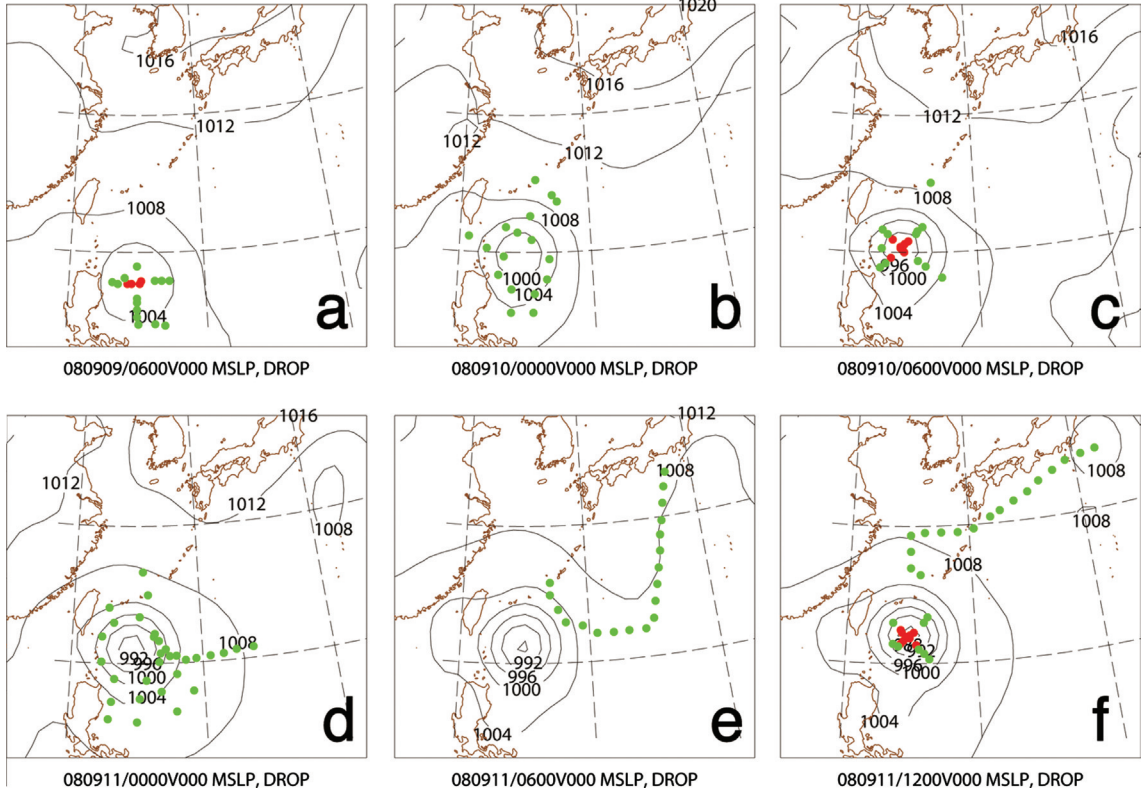


Fig. 4. Distribution of targeted dropsonde observations superposed with SLP (solid lines at 4 hPa intervals) of NCEP FNL at: (a) 0600 UTC 9; (b) 0000 UTC 10; (c) 0600 UTC 10; (d) 0000 UTC 11; (e) 0600 UTC 11; and (f) 1200 UTC 11 September 2008. The red dot represents observations within 100 km of the typhoon centre.

near the core region, an additional experiment ('CORE') was performed. The configuration of CORE was the same as that of EXP2, except that the CORE assimilation included the dropsonde observations near the inner-core region.⁵

The observational error statistics from NCEP were used for the conventional observations and the targeted dropsonde observations. The 0.3° (5 hPa) of observational error was assigned to TC position (minimum SLP) assimilation, based on Chen and Snyder (2006).

4. Results

4.1. Innovation statistics and rank histogram

In this subsection, the performance of the EnKF analysis scheme is evaluated with the innovation statistics⁶ and rank

histograms. The characteristics of the innovation statistics and rank histograms for all of the experiments were very similar, showing consistent performance of the EnKF analysis among experiments. Because the characteristics were similar, only the results of EXP3 for domain 1 were chosen for a more in-depth description.

Figure 5 shows the root-mean-square error (RMSE) spread, and bias of prior and posterior ensemble-mean fields. These innovation statistics were verified with respect to the radiosonde and dropsonde observations on the mandatory levels⁷ and accumulated for all analysis times. Vertical characteristics for RMSE, spread, and bias were quite similar between prior and posterior ensembles. The RMSEs of the wind fields had two peaks, one at the 200 hPa level and another at the 950 hPa level. The RMSE of temperature was large in the lower troposphere, with the largest peak near the upper boundary. Likewise, the RMSE of specific humidity was also large in the lower troposphere where the specific humidity was high.

⁵The core regions are defined as a circle with a radius of 100 km from the best track position.

⁶The innovation statistics is the statistics for the innovation. The innovation is defined as the difference of background fields from observations (Daley, 1991).

⁷These verifying data are not independent observations. Thus, we present the result of EXP3, which has a lower correlation between the assimilating and verifying data.

Table 2. Description of numerical experiments

Experiment	Description
EXP1	Assimilate the conventional observations.
EXP2	Assimilate the conventional observations and the targeted dropsonde observations.
EXP3	Assimilate the conventional observations and the TC position information.
EXP4	Assimilate the conventional observations, the TC position, and TC minimum SLP information.
EXP5	Assimilate the conventional observations, the targeted dropsonde observations, the TC position and TC minimum SLP information.
CORE	Same as EXP2, except that the dropsonde observations near the TC core regions are also assimilated here.

The biases of the wind fields were large in the upper troposphere, where the RMSEs were maximised. While warm and humid biases were evident in the lower troposphere, cold and dry biases were observed in the upper troposphere. Through the EnKF analysis, the RMSEs and biases of the ensemble-mean fields were reduced. The uncertainty of the posterior ensemble-mean represented by the ensemble spread was also reduced after analysis.

Note that, if the EnKF analysis is optimally performed, the innovation covariance should be equal to the sum of background error covariance and observational error covariance (Houtekamer et al., 2005; Whitaker et al., 2008):

$$E[(y^o - H\bar{x}^b)(y^o - H\bar{x}^b)^T] = HP^bH^T + R, \quad (1)$$

where y^o , \bar{x}^b , P^b , R , H , $E[\cdot]$, and T represent the observation, prior mean field, prior error covariance matrix, observational error covariance matrix, forward operator, expectation operator and transpose of a given matrix, respectively. Only the variance components (i.e. the diagonal components of the matrix) were evaluated here. The root mean of the diagonal components of the right-hand matrix of eq. (1) is defined as a predicted RMSE (Houtekamer et al., 2005; Meng and Zhang, 2008b), while that of the left-hand matrix is a prior RMSE. For the wind components (U and V), the prior and predicted RMSE were quite similar in the upper troposphere, while the prior RMSE was larger than the predicted RMSE in the lower troposphere (Fig. 5a,b). For the temperature component

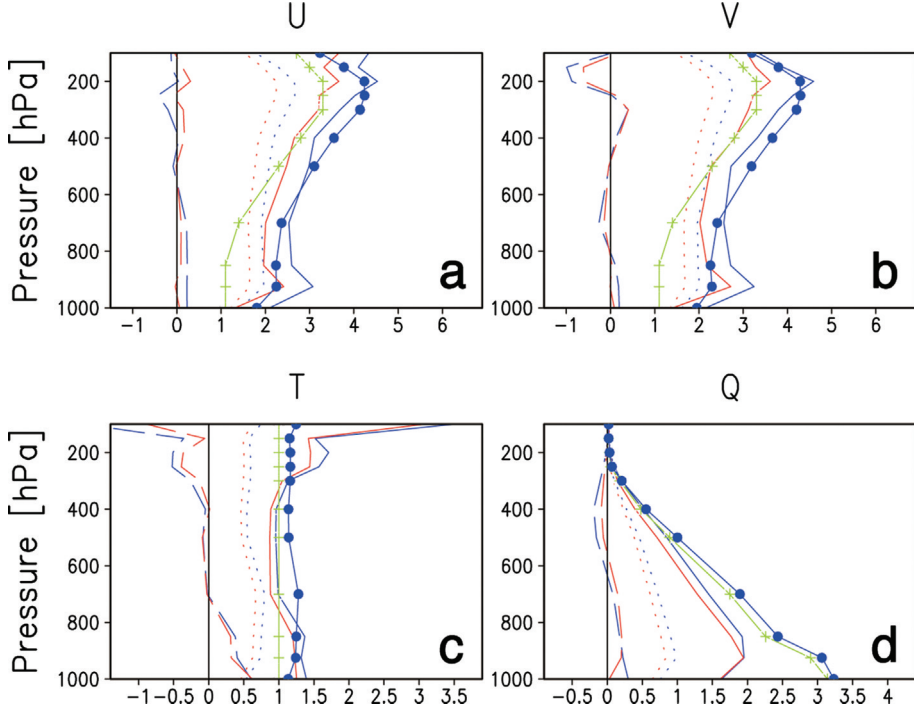


Fig. 5. The RMSE (solid lines), spread (dotted lines), bias (dashed lines) of prior (blue colored lines) and posterior (red colored lines) ensemble-mean fields accumulated for all analysis times for: (a) U ; (b) V ; (c) T ; and (d) Q components, verified via radiosonde and dropsonde observations in the mandatory levels. The observational error for each observational variable is denoted by a green line with cross marks, and the predicted RMSE is denoted by a blue line with closed circles.

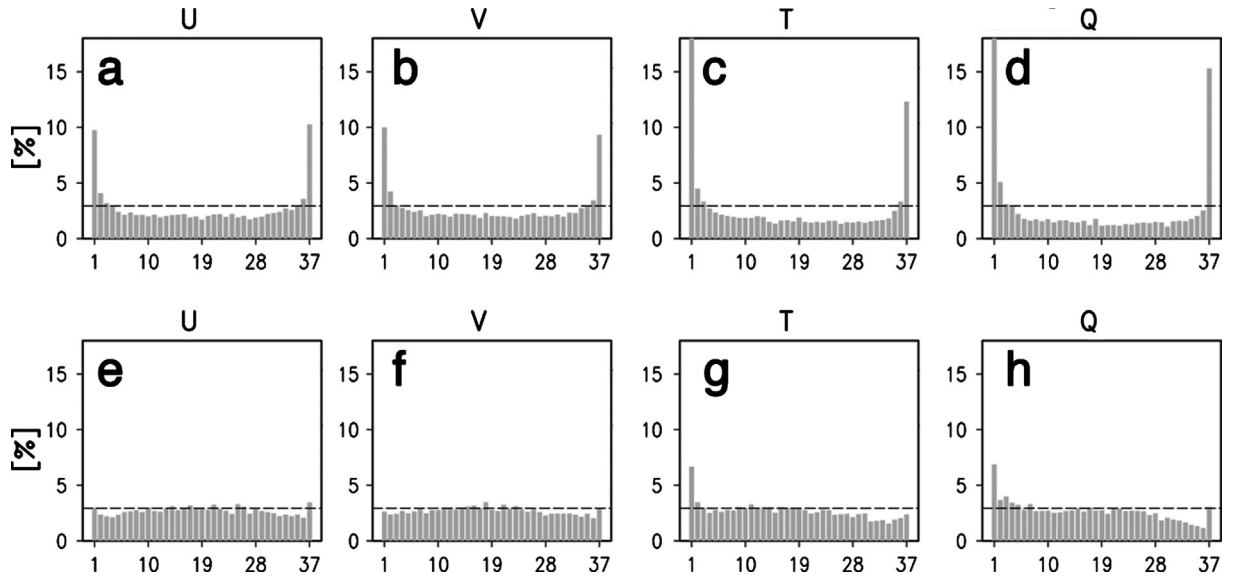


Fig. 6. Rank histograms of prior ensembles accumulated for all analysis times for: (a, e) U ; (b, f) V ; (c, g) T ; and (d, h) Q components, verified via radiosonde and dropsonde observations in the mandatory levels. The observational error is incorporated into the rank histograms in the lower panels (e–h). The dashed black lines denote the ideal value for the rank histograms (e.g., $100/37 = 2.70$).

(T), the predicted RMSE was larger in the mid-troposphere, while the prior RMSE was much larger in the upper troposphere (Fig. 5c). The large prior RMSE in the upper troposphere may be a consequence of the large cold bias in those levels. For the specific humidity component (Q), the predicted RMSE was greater than the prior RMSE over the entire troposphere (Fig. 5d).

Figure 6 shows the rank histograms (Hamill, 2001) for the prior ensembles accumulated for all analysis times, verified with respect to the radiosonde and dropsonde observations on the mandatory levels. A large spread is evident in the U-shaped rank histograms with two extreme ranks (Fig. 6a–d). The adjusted missing rates (Zhu et al., 1996; Hou et al., 2001; Meng and Zhang, 2008b) were 17, 17, 31 and 37% for the U , V , T , and Q components, respectively. These large positive adjusted missing rates represent the large ensemble spread. Hamill (2001) suggested that rank histograms should incorporate the observational error by adding random observational noise to the each ensemble realisation of observations. As incorporating the observational error (Fig. 6e–h), the extreme ranks were reduced significantly, and the rank histograms were flatter. The adjusted missing rates were also reduced to approximately 1.1, 0.1, 3.6 and 4.5% for U , V , T , and Q , respectively. These rank histograms can be considered ‘fairly flat’ since the adjusted missing rates were less than 10% (Hou et al., 2001; Meng and Zhang, 2008b). For T and Q , the rank histograms were skewed to the lower ranks, implying that there was an overall warm bias for T and a moist bias for Q .

From the innovation statistics and rank histogram, the EnKF analysis scheme performed reasonably well without a significant lack of ensemble spread, although the ensemble spread for wind variables was relatively small in the lower troposphere and there were some biases for thermal and moisture variables.

4.2. Examples of field change after EnKF analysis

Fig. 7 shows the ensemble-mean SLP of prior and posterior ensembles for EXP2 and EXP4 at the analysis time of 0000 UTC 11 September 2008. For domain 1 of EXP2 (Fig. 7a, b), the minimum SLP of the prior ensemble mean is about 987 hPa. The ensemble spread of the SLP is centred on the central position of the TC with the maximum value of 9.8 hPa. After EnKF assimilation of the conventional and targeted dropsonde observations, the minimum SLP of the posterior ensemble-mean slightly intensified to the value of 985 hPa, although the minimum SLP is far from that of best track (935 hPa). The ensemble spread that represents the uncertainty of given variable was also reduced, achieving a maximum value of 7.9 hPa. At this analysis time (0000 UTC 11), there were 31 targeted dropsonde observations around Sinlaku (Fig. 4d). These targeted dropsonde observations contributed to the intensified SLP field of Sinlaku. For domain 2 of EXP2 (Fig. 7c, d), the ensemble-mean SLP fields are deeper for both prior (986 hPa) and posterior (971 hPa) ensembles than those for domain 1. On the other hand, the ensemble spread is larger for both prior (13.1 hPa) and posterior

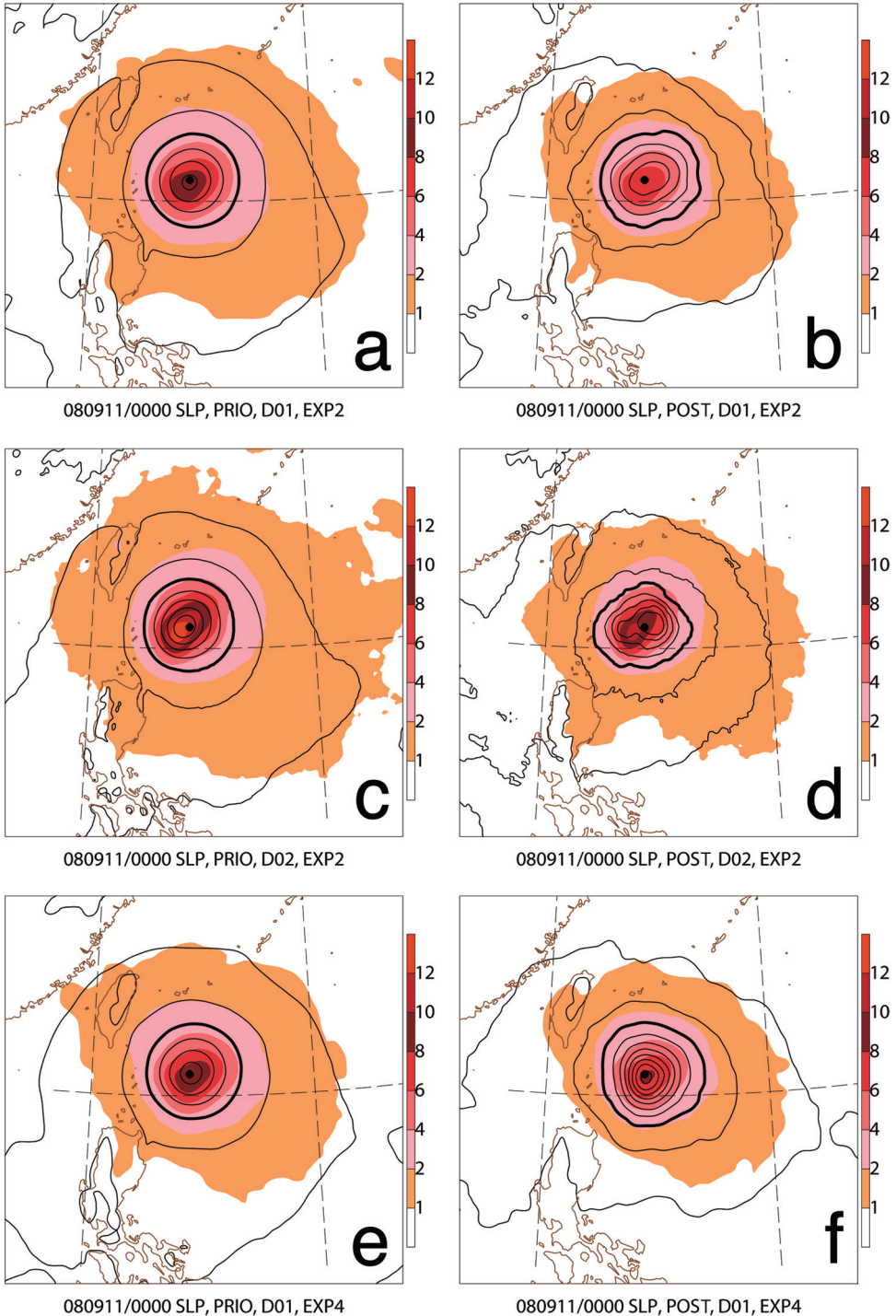


Fig. 7. The ensemble-mean SLP (solid lines at 4 hPa intervals) and corresponding spread (shaded region, hPa) of (a) prior and (b) posterior ensembles for domain 1 of EXP2 at 0000 UTC 11 September 2008, those of (c) prior and (d) posterior ensembles for domain 2 of EXP2, and those of (e) prior and (f) posterior ensembles for domain 1 of EXP4. The SLP of 1000 hPa is denoted by a thick solid line, and the best track position is indicated by a solid black dot in each figure.

(10.6 hPa) ensembles than those for domain 1 because a more intense structure of the SLP field was achieved from the fine resolution of domain 2, compared with that of

domain 1. Similar dependence of the ensemble spread on the horizontal resolution is reported by Buizza et al. (1998, 2003). Rather than deepening, the minimum SLP regions

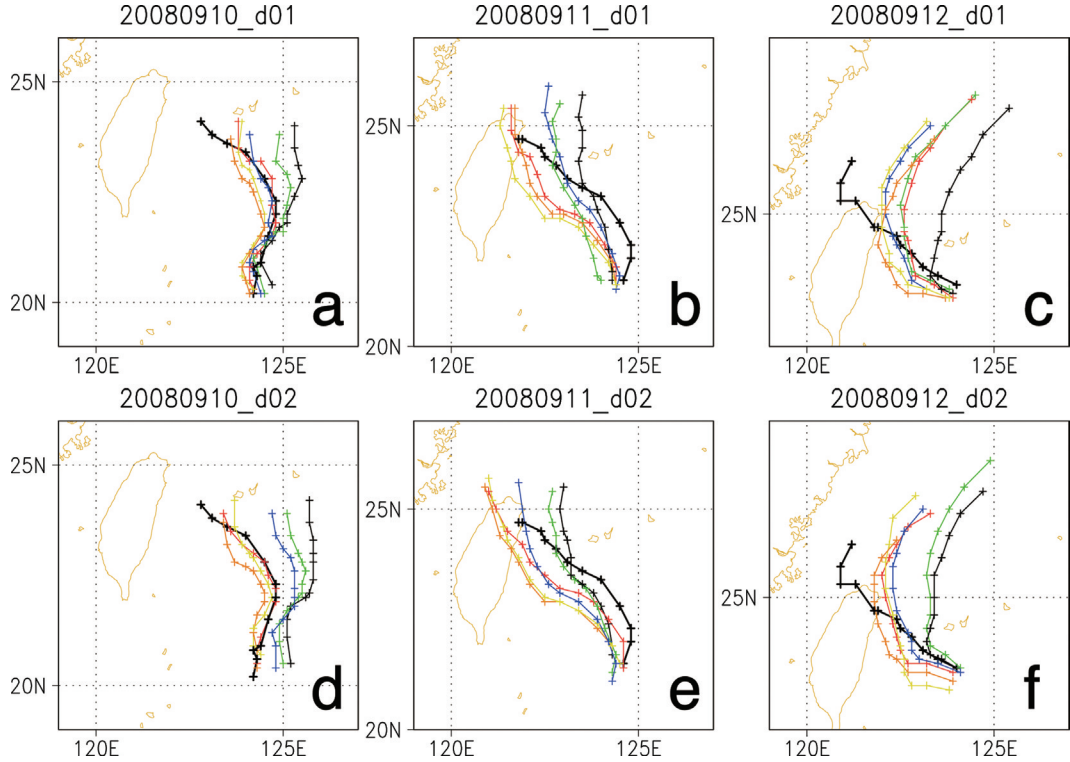


Fig. 8. Ensemble-mean tracks for domain 1 (upper panels) and domain 2 (lower panels) initiated at: (a, d) 0000 UTC 10; (b, e) 0000 UTC 11; and (c, f) 0000 UTC 12 September 2008. The lines represent the best track (thick black line), EXP1 (thin black line), EXP2 (red line), EXP3 (green line), EXP4 (blue line), EXP5 (orange line), and CORE (yellow line), respectively.

have shifted to the northeast in the posterior mean field of domain 2 (compare Fig. 7c, d). Interestingly, the pattern of the posterior spread is very similar to that of the prior spread, despite the movement of the minimum SLP regions. This similarity is a consequence of the covariance relaxation method (Zhang et al., 2004), which relaxes the posterior ensemble perturbations with the prior perturbations. The SLP fields of EXP4 are shown in Fig. 7e, f. The assimilation of SLP information of the best track efficiently produced the intense TC structure. Note that the minimum SLP of ensemble-mean field is deepened by approximately 15 hPa (from 985 to 971 hPa) for domain 1 by EnKF analysis procedure. For domain 2, the minimum SLP of ensemble-mean field is also intensified by approximately 23 hPa (from 975 to 952 hPa, not shown).

4.3. Evaluation of ensemble-mean forecast track

Figure 8a–c show the ensemble-mean tracks of a 3-day forecast for domain 1, initiated at 0000 UTC 10, 11 and 12 September 2008. The time-averaged ensemble-mean track errors are shown in Fig. 9. For track forecasts initiated at 0000 UTC 10 (Fig. 8a), EXP1 showed a northward track after a 36-h forecast time, failed to

reproduce the northwestward movement of the best track. Additional assimilation of the targeted dropsonde observations (EXP2) improved the initial position of Sinlaku compared to EXP1. The initial position error was reduced from 58 km in EXP1 to 33 km in EXP2. The EXP2 also improved the northwestward track after 36 hours forecast time (Fig. 8a). As a result, the time-averaged track error of EXP2 was reduced to one-third of that of EXP1 (Fig. 9a). The TC position assimilation (EXP3) slightly improved the initial TC location and track forecast, although the northward track after the 36-h forecast time was not significantly improved (Fig. 8a and 9a). The additional assimilation of the TC position and minimum SLP information (EXP4) resulted in an initial position error of 35 km. The reduction of the time-averaged track error of EXP4 was as much as 38% of that of EXP1 (and 16% of that of EXP3). Although the lowest initial position error (23 km) is found in EXP5, the time-averaged track error for EXP5 is larger than for EXP2, owing to the southwestward deflection of the forecast track in EXP5 (Fig. 8a and 9a).

For the track forecast initiated at 0000 UTC 11 September 2008 (Fig. 8b), all of the experiments showed straight movements toward the north or northwest, and failed to represent the initial clockwise recurvature of the best track.

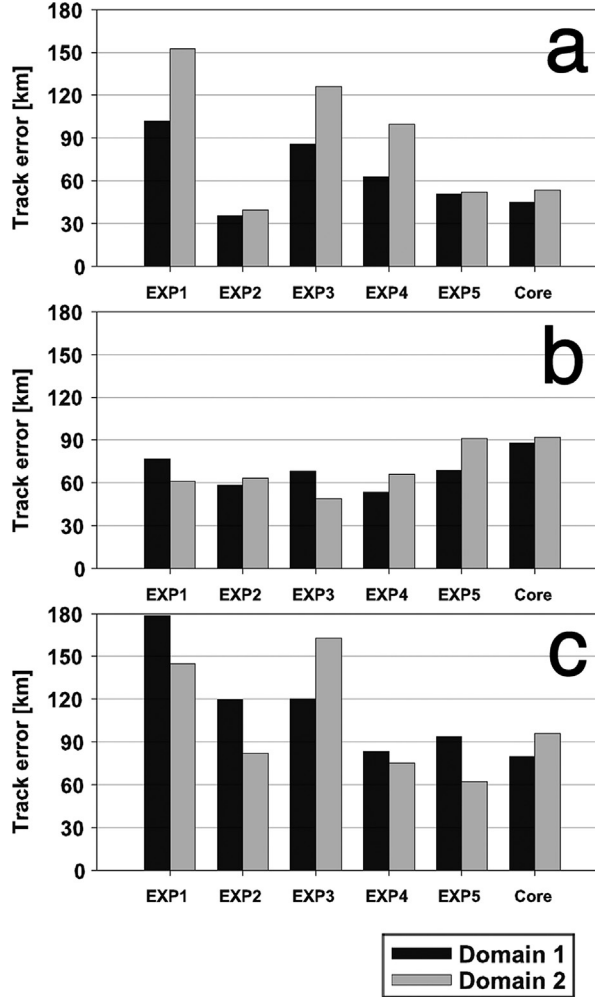


Fig. 9. Seventy two-hour averaged forecast errors (km) of ensemble-mean tracks for the indicated experiments initiated at: (a) 0000 UTC 10; (b) 0000 UTC 11; and (c) 0000 UTC 12 September 2008.

EXP1, EXP3, and EXP4 showed northward movement while EXP2, EXP5 showed northwestward movement. Consequently, the overall patterns of the forecast tracks were better represented by assimilating the targeted dropsonde observations, despite the southwestward biases in the forecast tracks compared to the best track (Fig. 8b). The time-averaged forecast track errors for EXP2 and EXP4 were substantially reduced compared to those for EXP1 (Fig. 9b). For the track forecast initiated at 0000 UTC 12 September 2008 (Fig. 8c), all of the experiments showed the early-recurving tracks. EXP1 started to recurve toward the northeast at the 12-h forecast time, which resulted in a large time-averaged track error of 180 km. The additional assimilation of targeted dropsonde observations, TC position, and minimum SLP information, both separately and all together, reduced the time-averaged track error, although the time of the TC recurvature was still early compared to that of the best track (Fig. 8c and 9c).

Figure 8d–f show ensemble-mean tracks of the 3-day forecast for domain 2, initiated at 0000 UTC 10, 11 and 12 September 2008. The overall observational effects found in domain 2 are similar to those discussed above for domain 1. For the track forecast initiated at 0000 UTC 10 September 2008 (Fig. 8d), EXP1 had a larger initial position error (92 km) in domain 2 than in domain 1 (compare Fig. 8a,b), and the time-averaged track error for domain 2 was also larger than that for domain 1 (Fig. 9a). However, the assimilation of targeted dropsonde observations (EXP2, EXP5) improved the initial position as well as the track forecast in domain 2 (Fig. 8d and 9a). In fact, the average track error of EXP1 was reduced by as much as 79% for EXP2 and 77% for EXP5 (Fig. 9a). The assimilation of TC position and minimum SLP information also improved the track forecast, although there were still relatively northward deflections as in EXP1 (Fig. 8d). For the forecast track initiated at 0000 UTC 11 September

Table 3. Differences (upper and left experiment) of time-averaged track errors between the major experiments shown in Fig. 9

Initiation time	Domain	Experiment	EXP2	EXP3	EXP4	EXP5	CORE
0000 UTC 10 September 2008	Domain 1	EXP1	-66.7	-16.4	-39.1	-51.2	-57.1
		EXP2				15.5	9.6
		EXP3			-22.7		
	Domain 2	EXP1	-113.0	-26.6	-53.0	-100.4	-99.3
		EXP2				12.6	13.7
		EXP3			-26.5		
0000 UTC 11 September 2008	Domain 1	EXP1	-18.3	-8.4	-23.5	-7.8	11.2
		EXP2				10.6	29.6
		EXP3			-15.1		
	Domain 2	EXP1	2.5	-12.0	5.2	30.0	31.3
		EXP2				27.5	28.8
		EXP3			17.2		
0000 UTC 12 September 2008	Domain 1	EXP1	-59.0	-58.6	-95.3	-85.0	-98.7
		EXP2				-26.0	-39.7
		EXP3			-36.7		
	Domain 2	EXP1	-63.2	17.8	-69.6	-82.7	-48.9
		EXP2				-19.4	14.3
		EXP3				-87.5	

The bold (italic) numbers are within the 95% (90%) confidence interval, after implementing the paired *t*-test.

2008 (Fig. 8e), the domain 2 tracks showed north to northwestward movement similar to those for domain 1. The initial position error was greatly reduced by including the targeted dropsonde assimilation (down to 13 km for EXP2 and 7 km for EXP5), when compared with that of EXP1 (46 km). Despite a systematic southwestward departure, the additional assimilation of targeted dropsonde observations (EXP2, EXP5) and minimum SLP information (EXP4) improved the initial counter-clockwise recurvature and northwestward track. For the domain 2 track forecast initiated at 0000 UTC 12 September 2008 (Fig. 8f), all of the experiments showed early northward movement, which can also be seen in domain 1. Furthermore, the assimilation of targeted dropsonde observations and TC minimum SLP information reduced the time-averaged track error (Fig. 9c).

The major differences between the time-averaged track error of the various experiments are shown with 90 and 95% confidence levels after implementing the paired *t*-test in Table 3. Compared to the reference experiment (i.e. EXP1), the additional assimilation of the targeted dropsonde and TC information (i.e. EXP2, 3, 4 and 5) reduced the time-averaged forecast track errors. The impact of the additional assimilations was notably significant for the forecasts at 0000 UTC 10 and 12 September 2008. On the other hand, when the conventional observations and targeted dropsonde observations were assimilated (i.e.

EXP2), the additional assimilation of TC best track information degraded (i.e. increased the error of) the track forecast (compare EXP2 and EXP5 in Table 3), except for the 0000 UTC 12 initiation time.⁸ When the conventional observations and TC position information were assimilated (i.e. EXP3), the additional assimilation of TC minimum SLP information significantly improved the track forecast (compare EXP3 and EXP4 in Table 3) and efficiently analysed the intense TC structures (e.g. Fig. 7f). The importance of using intensity information for TC predictions has also been reported in the BDA studies (Xiao et al., 2000, 2006). Overall, the effect of additional observations on the track errors initialised at 0000 UTC 11 September 2008 were less significant (and the differences among the experiments were also smaller) than those initialised at other times. This result may be a consequence of the relatively simple, large-scale features occurring at the 0000 UTC 11 initiation time. On the other hand, the complicated, rapidly-developing track for the 0000 UTC 10 initiation time and the interaction with mid-latitude weather systems and high mountains over Taiwan for the 0000 UTC 12 initiation time, may have complicated the effect of incorporating additional observations.

⁸Because there were no dropsonde observations for the analysis time of 0000 UTC 12 September 2008, the average track error for EXP5 is smaller than that for EXP2.

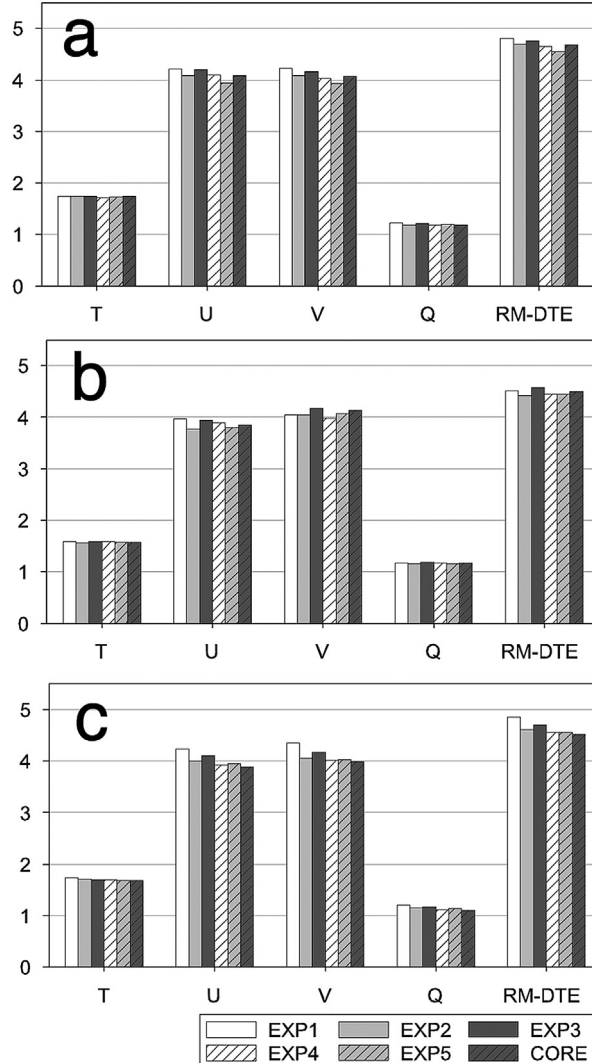


Fig. 10. Seventy two-hour averaged RMSE of ensemble-mean forecast fields for experiments initiated at: (a) 0000 UTC 10; (b) 0000 UTC 11; and (c) 0000 UTC 12 September 2008. The forecast fields are verified with radiosonde and dropsonde observations in the mandatory levels. The units for T , U , V , Q , and RM-DTE are K, m s^{-1} , m s^{-1} , g kg^{-1} and m s^{-1} , respectively.

4.4. Evaluation of ensemble-mean forecasts compared with observations

In this subsection, the ensemble-mean fields of 3-day forecasts are evaluated with respect to the radiosonde and targeted dropsonde observations.⁹ While the TC track is generally the most important forecast measure, the ensemble forecast fields that do not directly represent the TC parameters (e.g. track, maximum wind, and minimum SLP) are also informative. Owing to the small observational coverage of the radiosonde network for domain 2, the statistics were only derived here for

domain 1. Figure 10 shows the time-averaged RMSE for each variable and initiation time. The momentum variables appeared to vary more than thermal and moisture variables. To measure the overall RMSE for most of the variables, the difference total energy (DTE) was defined as in Zhang (2005):

$$\text{DTE} = \frac{1}{2} \left(u'u' + v'v' + \frac{C_p}{T_r} T'T' \right), \quad (2)$$

where C_p is $1004.7 \text{ J kg}^{-1} \text{ K}^{-1}$, the reference temperature T_r is 290 K , and the primed variables denote the differences between the observations and the ensemble forecast mean fields. The root mean of DTE (RM-DTE) is also presented in Fig. 10.

⁹As in Section 4.1, these verifying observations are not the independent observations.

Table 4. The rejection rate (%), total number of observations, and number of corresponding soundings of dropsonde observations for six analysis times (see Fig. 4)

		0600 UTC 9 September 2008	0000 UTC 10	0600 UTC 10	0000 UTC 11	0600 UTC 11	1200 UTC 11
For CORE experiment							
Inner-core region	Rejection rate (%)	26.8	–	36.0	–	–	48.0
	Total no. of observations (no. of soundings)	112 (4)	–	272 (9)	–	–	352 (11)
Outside region	Rejection rate (%)	14.5	3.3	21.3	1.9	0.2	4.8
	Total no. of observations (no. of soundings)	470 (14)	1337 (17)	418 (12)	2187 (31)	1433 (19)	1683 (25)
Total dropsonde	Rejection rate (%)	16.8	3.3	27.1	1.9	0.2	12.3
	Total no. of observations (no. of soundings)	582 (18)	1337 (17)	690 (21)	2187 (31)	1433 (19)	2035 (36)

For the ensemble forecast initiated at 0000 UTC 10 September 2008 (Fig. 10a), the positive effects of the targeted dropsonde observations (EXP2), TC position (EXP3) and minimum SLP information (EXP4) can be seen. Note that EXP5, which assimilated all observations, presented the smallest RM-DTE. For the ensemble forecast initiated at 0000 UTC 11 September 2008 (Fig. 10b), the variation of the RM-DTE among the experiments is smaller than the variation of the ensemble forecasts initiated at both 0000 UTC 10 and 0000 UTC 12 (Fig. 10a, c). Also, the mean value of the RM-DTE for all of the experiments (4.48 m s^{-1}) is slightly smaller¹⁰ than the mean RM-DTE of just those initiated at 0000 UTC 10 (4.69 m s^{-1}) and 0000 UTC 11 (4.64 m s^{-1}). This result is related to the relatively simple, straight-moving track found 24 h after the 0000 UTC 11 initiation time. For the forecast initiated at 0000 UTC 10, the best track shows a complex track moving clockwise for the first 36 h and then counter-clockwise for the next 36 h. For the forecast initiated at 0000 UTC 12, the ensemble-mean forecast tracks showed an early recurvature compared with the best track, which made landfall on Taiwan and then recurved after interacting with the mid-latitude systems. For the ensemble forecast initiated at 0000 UTC 12 (Fig. 10c), the positive effects of the targeted dropsonde, TC position and minimum SLP information can also be seen.

4.5. Effect of core dropsonde observations

To determine the effect of the assimilation of inner-core targeted dropsonde observations, the additional experiment ‘CORE’ was implemented. Table 4 shows the

rejection rate of dropsonde observations during the EnKF analysis procedure for domain 1¹¹ of CORE. Note that, before assimilating the observations, there is a simple data quality control (QC) process that rejects the observation if the innovation is larger than five times of the observational error assumed. The rejection rate of the dropsonde observations in the inner-core region was larger than the region outside of the core. The overall rejection rate was also larger for the operations that observed TC structures crossing the inner-core region (Fig. 4a, c, f and Table 4). This increased rejection rate occurred primarily because the eyewall and inner-core structure of the TC were not represented well in the current modelling systems (of 45 and 15 km resolution). Thus, many dropsonde observations causing large innovations over the inner-core region were regarded as erroneous information and rejected in the assimilation system. Most (about 99%) of the rejected components of the dropsonde observations were wind components, owing to their large variation near the TC centre relative to the variations of the thermal and moisture components. The time-averaged track errors of CORE were larger than those of EXP2, which did not assimilate the core observations. The assimilation of inner-core observations significantly degraded the forecast initiated at 0000 UTC 10 and 0000 UTC 11 September 2008 (Table 3) because the configuration of the current modelling and data assimilation system could not feasibly resolve the detailed structure of the observations over the core region.

5. Summary and discussion

In this study, a series of observing system experiments (OSEs) with a WRF-based EnKF system were performed

¹⁰These differences are not significant.

¹¹The rejection rate of dropsonde observations for domain 2 is similar to that for domain 1.

for the TC Sinlaku (2008), an extensively observed storm during T-PARC. Conventional data, targeted dropsonde observations from T-PARC, and the position and minimum SLP information from the RSMC Tokyo best track were used for the OSEs. Innovation statistics and rank histograms were used to evaluate the performance of the EnKF analysis scheme. By conducting the EnKF analysis, the RMSEs and biases of the ensemble-mean fields, as well as the uncertainty of the ensembles were all reduced. The spread of the prior ensemble was reasonably maintained since the prior RMSE and the predicted RMSE are comparable. From the rank histograms that incorporated the observational error, it was evident that the rank histograms were fairly flat with adjusted missing rates of less than 10%, although an overall warm bias for T and a moist bias for Q could be seen.

The ensemble-mean forecast tracks of the experiments were explored to evaluate the effect of assimilating each observation type, with a focus on the impacts to the TC track forecast. EXP1, which only assimilated the conventional observations, failed to represent the northwestward track after the 36-h forecast initiated at 0000 UTC 10 September 2008. The additional assimilation of the targeted dropsonde observations (EXP2) reduced the initial TC position error and improved the northwestward track after the 36-h forecast. Similarly, the additional assimilation of TC position data (EXP3) from the RSMC Tokyo best track slightly improved the initial TC location and track forecast. The assimilation of minimum SLP information (EXP4) also improved the track forecast. For the track forecast initiated at 0000 UTC 11 September 2008, the assimilation of targeted dropsonde observations (EXP2 and EXP5) showed similar northwestward movement toward the best track, despite the southwestward departure. For the track forecast initiated at 0000 UTC 12 September, the assimilation of targeted dropsonde observations (EXP2 and EXP5) and minimum SLP information (EXP4) reduced the time-averaged track error, compared to that of EXP1. The effect of the dropsonde assimilation over the TC core region was evaluated via an additional experiment, CORE. Through a QC procedure, about 30–50% of the core dropsonde observations were rejected, especially in the wind components, because the current modelling system could not resolve the intense TC structure used as the first-guess in the data assimilation. The track forecast for CORE was significantly degraded compared to that for EXP2 (without core assimilation) at the initiation times of 0000 UTC 10 and 11 September 2008.

The ensemble-mean fields of 3-day forecasts were evaluated with respect to the radiosonde and targeted dropsonde observations. The variation of the average forecast errors (i.e. RM-DTE) for the experiments were different

for each forecast initiation time. In particular, the forecast tracks were more variable if the typhoon developed rapidly or interacts with other systems, showing complex tracks. For example, the track at an initiation time of 0000 UTC 10 September 2008 that rapidly developed and the track 0000 UTC 12 September 2008 that interacted with mid-latitude weather systems and high-altitude mountains both had more variable forecast tracks.

The current study reaffirms that the targeted dropsonde observations contributed to the analysis of the initial TC track position as well as to the subsequent TC track forecasts in the EnKF data assimilation system. The assimilation of location and intensity information of the TC track was also helpful for the analysis and forecast of the track, especially when targeted dropsonde observations did not exist. The assimilation of dropsonde observations over the inner-core region degraded the track forecast for the initiation times of 0000 UTC 10 and 11 September 2008, likely due to the use of insufficient model resolution as well as the representativeness error of the dropsonde observations inside core area. As mentioned in Aberson (2008), and Harnisch and Weissmann (2010), more advanced data assimilation systems and more sophisticated QC procedures may be vital to improve the function and efficiency of dropsonde observations over TC core regions. Ongoing and future research seeks to extend the current findings to more cases and to perform OSEs at cloud-resolving resolution, the two key limitations in the current study.

6. Acknowledgements

The authors thank two anonymous reviewers for their valuable comments. This study was supported by the Korea Meteorological Administration Research and Development Program under Grant CATER 2006-2102. The authors acknowledge Zhiyong Meng and Yonghui Weng for help on the WRF-EnKF system. The authors also appreciate the DOTSTAR and THORPEX T-PARC programs for the dropsonde data.

References

- Aberson, S. D. 2002. Two years of operational hurricane synoptic surveillance. *Wea. Forecast.* **17**, 1101–1110.
- Aberson, S. D. 2003. Targeted observations to improve operational tropical cyclone track forecast guidance. *Mon. Wea. Rev.* **131**, 1613–1628.
- Aberson, S. D. 2008. Large forecast degradations due to synoptic surveillance during the 2004 and 2005 hurricane seasons. *Mon. Wea. Rev.* **136**, 3138–3150.

- Aberson, S. D. 2010. 10 years of Hurricane Synoptic Surveillance (1997–2006). *Mon. Wea. Rev.* **138**, 1536–1549.
- Aberson, S. D. and Etherton, B. J. 2006. Targeting and data assimilation studies during Hurricane Humberto (2001). *J. Atmos. Sci.* **63**, 175–186.
- Aberson, S. D. and Franklin, J. L. 1999. Impact on hurricane track and intensity forecasts of GPS dropwindsonde observations from the first-season flights of the NOAA Gulfstream-IV jet aircraft. *Bull. Am. Meteorol. Soc.* **80**, 421–427.
- Aberson, S. D., Majumdar, S. J., Reynolds, C. A. and Etherton, B. J. 2011. An observing system experiment for tropical cyclone targeting techniques using the Global Forecast System. *Mon. Wea. Rev.* **139**, 895–907.
- Aksoy, A., Dowell, D. C. and Snyder, C. 2009. A multicase comparative assessment of the ensemble Kalman filter for assimilation of radar observations. Part I: Storm-scale analyses. *Mon. Wea. Rev.* **137**, 1805–1824.
- Anthes, R. A., Ector, D., Hunt, D. C., Kuo, Y.-H., Rocken, C. and co-authors. 2008. The COSMIC/FORMOSAT-3 Mission: early results. *Bull. Am. Meteorol. Soc.* **89**, 313–333.
- Betts, A. K. 1986. A new convective adjustment scheme. Part I: observational and theoretical basis. *Quart. J. R. Meteorol. Soc.* **112**, 677–691.
- Betts, A. K. and Miller, M. J. 1986. A new convective adjustment scheme. Part II: single column tests using GATE wave, BOMEX, ATEX and Arctic air-mass data sets. *Quart. J. R. Meteorol. Soc.* **112**, 693–709.
- Bishop, C. H., Etherton, B. J. and Majumdar, S. J. 2001. Adaptive sampling with the ensemble transform Kalman filter. Part I: theoretical aspects. *Mon. Wea. Rev.* **129**, 420–435.
- Bormann, N., Saarinen, S., Kelly, G. and Thépaut, J.-N. 2003. The spatial structure of observation errors in atmospheric motion vectors from geostationary satellite data. *Mon. Wea. Rev.* **131**, 706–718.
- Buizza, R., Cardinali, C., Kelly, G. and Thépaut, J.-N. 2007. The value of observations. II: the value of observations located in singular-vector-based target areas. *Quart. J. R. Meteorol. Soc.* **133**, 1817–1832.
- Buizza, R., Petroliagis, T., Palmer, T., Barkmeijer, J., Hamrud, M. and co-authors. 1998. Impact of model resolution and ensemble size on the performance of an Ensemble Prediction System. *Quart. J. R. Meteorol. Soc.* **114**, 1935–1960.
- Buizza, R., Richardson, D. S. and Palmer, T. N. 2003. Benefits of increased resolution in the ECMWF ensemble system and comparison with poor-man's ensembles. *Quart. J. R. Meteorol. Soc.* **129**, 1269–1288.
- Burpee, R. W., Aberson, S. D., Franklin, J. L., Lord, S. J. and Tuleya, R. E. 1996. The impact of omega dropwindsondes on operational hurricane track forecast models. *Bull. Am. Meteorol. Soc.* **77**, 925–933.
- Chen, F. and Dudhia, J. 2001. Coupling an advanced land surface–hydrology model with the Penn State–NCAR MM5 modeling system. Part II: model implementation and sensitivity. *Mon. Wea. Rev.* **129**, 569–585.
- Chen, Y. and Snyder, C. 2006. Initializing a hurricane vortex with an ensemble Kalman filter. In: Proceedings of the *Seventh WRF Users Workshop*, Boulder, CO, Preprints. Online at: www.mmm.ucar.edu/wrf/users/workshops/WS2006/abstracts/Session03/3_3_Chen.pdf.
- Chen, Y. and Snyder, C. 2007. Assimilation vortex position with an ensemble Kalman filter. *Mon. Wea. Rev.* **135**, 1828–1845.
- Chou, K.-H. and Wu, C.-C. 2008. Development of the typhoon initialization in a mesoscale model – combination of the bogus vortex with the dropwindsonde data in DOTSTAR. *Mon. Wea. Rev.* **136**, 865–879.
- Chou, K.-H., Wu, C.-C., Lin, P.-H., Aberson, S. D., Weissmann, M. and co-authors. 2011. The impact of dropwindsonde observations on typhoon track forecasts in DOTSTAR and T-PARC. *Mon. Wea. Rev.* **139**, 1728–1743.
- Daley, R. 1991. *Atmospheric Data Analysis*. Cambridge University Press. New York, USA, 457 pp.
- Dudhia, J. 1989. Numerical study of convection observed during the Winter Monsoon Experiment using a mesoscale two-dimensional model. *J. Atmos. Sci.* **46**, 3077–3107.
- Elsberry, R. L. and Harr, P. A. 2008. Tropical cyclone structure (TCS08) field experiment science basis, observational platforms, and strategy. *Asia-Pacific J. Atmos. Sci.* **44**, 209–231.
- Evensen, G. 1994. Sequential data assimilation with a nonlinear quasi-geostrophic model using Monte Carlo methods to forecast error statistics. *J. Geophys. Res.* **99**, 10143–10162.
- Gaspari, G. and Cohn, S. E. 1999. Construction of correlation functions in two and three dimensions. *Quart. J. R. Meteorol. Soc.* **125**, 723–757.
- Grell, G. A. 1993. Prognostic evaluation of assumptions used by cumulus parameterizations. *Mon. Wea. Rev.* **121**, 764–787.
- Grell, G. A. and Devenyi, D. 2002. A generalized approach to parameterizing convection combining ensemble and data assimilation techniques. *Geophys. Res. Lett.* **29**, 1693. doi:10.1029/2002GL015311.
- Hamill, T. M. 2001. Interpretation of rank histograms for verifying ensemble forecasts. *Mon. Wea. Rev.* **129**, 550–560.
- Hamill, T. M., Whitaker, J. S., Fiorino, M. and Benjamin, S. G. 2011. Global ensemble predictions of 2009’s tropical cyclones initialized with an ensemble Kalman filter. *Mon. Wea. Rev.* **139**, 668–688.
- Hamill, T. M., Whitaker, J. S. and Snyder, C. 2001. Distance-dependent filtering of background error covariance estimates in an ensemble Kalman filter. *Mon. Wea. Rev.* **129**, 2776–2790.
- Harnisch, F. and Weissmann, M. 2010. Sensitivity of typhoon forecasts to different subsets of targeted dropsonde observations. *Mon. Wea. Rev.* **138**, 2664–2680.
- Hong, S.-Y., Dudhia, J. and Chen, S.-H. 2004. A revised approach to ice microphysical processes for the parameterization of clouds and precipitation. *Mon. Wea. Rev.* **132**, 103–120.
- Hong, S.-Y. and Lim, J.-O. 2006. The WRF single-moment 6-class microphysics scheme (WSM6). *J. Korean Meteorol. Soc.* **42**, 129–151.
- Hong, S.-Y., Noh, Y. and Dudhia, J. 2006. A new vertical diffusion package with an explicit treatment of entrainment processes. *Mon. Wea. Rev.* **134**, 2318–2341.
- Hou, D., Kalnay, E. and Drogemeier, K. K. 2001. Objective verification of the SAMEX’98 ensemble forecasts. *Mon. Wea. Rev.* **128**, 73–91.

- Houtekamer, P. L. and Mitchell, H. L. 2001. A sequential ensemble Kalman filter for atmospheric data assimilation. *Mon. Wea. Rev.* **129**, 123–137.
- Houtekamer, P. L., Mitchell, H. L., Pellerin, G., Buehner, M., Charron, M. and co-authors. 2005. Atmospheric data assimilation with an ensemble Kalman filter: results with real observations. *Mon. Wea. Rev.* **133**, 604–620.
- Hsiao, L.-F., Liou, C.-S., Yeh, T.-C., Guo, Y.-R., Chen, D.-S. and co-authors. 2010. A vortex relocation scheme for tropical cyclone initialization in Advanced Research WRF. *Mon. Wea. Rev.* **138**, 3298–3315.
- Huang, C.-Y., Kuo, Y.-H., Chen, S.-H. and Vandenberghe, F. 2005. Improvements in typhoon forecast with assimilated GPS occultation refractivity. *Wea. Forecast.* **20**, 931–953.
- Janjić, Z. I. 1994. The step-mountain Eta coordinate model: further developments of the convection, viscous sub-layer, and turbulence closure schemes. *Mon. Wea. Rev.* **122**, 927–945.
- Janjić, Z. I. 2002. Nonsingular implementation of the Mellor–Yamada level 2.5 scheme in the NCEP Meso model. NCEP Office Note 437, 61 pp.
- Jung, B.-J., Kim, H. M., Kim, Y.-H., Jeon, E.-H. and Kim, K.-H. 2010. Observation system experiments for Typhoon Jangmi (200815) observed during T-PARC. *Asia-Pacific J. Atmos. Sci.* **46**, 305–316.
- Kain, J. S. 2004. The Kain–Fritsch convective parameterization: an update. *J. Appl. Meteorol.* **43**, 170–181.
- Kain, J. S. and Fritsch, J. M. 1993. Convective parameterization for mesoscale models: the Kain–Fritsch scheme. In: *The Representation of Cumulus Convection in Numerical Models* (eds. K. A. Emanuel and Raymond D. J.). American Meteorological Society Monograph, Boston, USA, 246 pp.
- Kaplan, J. and DeMaria, M. 2003. Large-scale characteristics of rapidly intensifying tropical cyclones in the North Atlantic basin. *Wea. Forecast.* **18**, 1093–1108.
- Kim, H. M. and Jung, B.-J. 2009a. Singular vector structure and evolution of a recurring tropical cyclone. *Mon. Wea. Rev.* **137**, 505–524.
- Kim, H. M. and Jung, B.-J. 2009b. Influence of moist physics and norms on singular vectors for a tropical cyclone. *Mon. Wea. Rev.* **137**, 525–543.
- Kim, H. M. and Morgan, M. C. 2002. Dependence of singular vector structure and evolution on the choice of norm. *J. Atmos. Sci.* **59**, 3099–3116.
- Kurihara, Y., Bender, M. A., Tuleya, R. E. and Ross, R. J. 1995. Improvements in the GFDL hurricane prediction system. *Mon. Wea. Rev.* **121**, 2030–2045.
- Langland, R. H. 2005. Issues in targeted observing. *Quart. J. R. Meteorol. Soc.* **131**, 3409–3425.
- Langland, R. H., Velden, C., Pauley, P. M. and Berger, H. 2009. Impact of satellite-derived rapid-scan wind observations on numerical model forecasts of Hurricane Katrina. *Mon. Wea. Rev.* **137**, 1615–1622.
- Lin, Y.-L., Farley, R. D. and Orville, H. D. 1983. Bulk parameterization of the snow field in a cloud model. *J. Climate Appl. Meteorol.* **22**, 1065–1092.
- Majumdar, S. J., Aberson, S. D., Bishop, C. H., Buiizza, R., Peng, M. S. and co-authors. 2006. A comparison of adaptive observing guidance for Atlantic tropical cyclones. *Mon. Wea. Rev.* **134**, 2354–2372.
- Mellor, G. L. and Yamada, T. 1982. Development of a turbulence closure model for geophysical fluid problems. *Rev. Geophys.* **20**, 851–875.
- Meng, Z. and Zhang, F. 2007. Test of an ensemble Kalman filter for mesoscale and regional-scale data assimilation. Part II: imperfect model experiments. *Mon. Wea. Rev.* **135**, 1403–1423.
- Meng, Z. and Zhang, F. 2008a. Test of an ensemble Kalman filter for mesoscale and regional-scale data assimilation. Part III: comparison with 3DVAR in a real-data case study. *Mon. Wea. Rev.* **136**, 522–540.
- Meng, Z. and Zhang, F. 2008b. Test of an ensemble Kalman filter for mesoscale and regional-scale data assimilation. Part IV: performance over a warm-season month of June 2003. *Mon. Wea. Rev.* **136**, 3671–3682.
- Meng, Z. and Zhang, F. 2011. Limited area ensemble based data assimilation: a review. *Mon. Wea. Rev.* **139**, 2025–2045.
- Mlawer, E. J., Taubman, S. J., Brown, P. D., Iacono, M. J. and Clough, S. A. 1997. Radiative transfer for inhomogeneous atmosphere: RRTM, a validated correlated-k model for the long-wave. *J. Geophys. Res.* **102D**, 16663–16682.
- Noh, Y., Cheon, W. G., Hong, S.-Y. and Raasch, S. 2003. Improvement of the K-profile model for the planetary boundary layer based on large eddy simulation data. *Bound. Layer Meteorol.* **107**, 401–427.
- Palmer, T. N., Gelaro, R., Barkmeijer, J. and Buiizza, R. 1998. Singular vectors, metrics and adaptive observations. *J. Atmos. Sci.* **55**, 633–653.
- Parsons, D., Harr, P., Nakazawa, T., Jones, S. and Weissmann, M. 2008. An overview of the THORPEX – Pacific Asian Regional Campaign (T-PARC) during August–September 2008. *Proceedings of the 28th Conference on Hurricanes and Tropical Meteorology*, Orlando, FL, AMS, 1–6.
- Peng, M. S. and Reynolds, C. A. 2006. Sensitivity of tropical cyclone forecasts as revealed by singular vectors. *J. Atmos. Sci.* **63**, 2508–2528.
- Pu, Z.-X. and Braun, S. A. 2001. Evaluation of bogus vortex techniques with four-dimensional variational data assimilation. *Mon. Wea. Rev.* **129**, 2023–2039.
- Pu, Z.-X., Li, X., Velden, C. S., Aberson, S. D. and Lui, W. T. 2008. The impact of aircraft dropsonde and satellite wind data on numerical simulations of two landfalling tropical storms during the Tropical Cloud Systems and Processes Experiment. *Wea. Forecast.* **23**, 62–79.
- Rabier, F., Gauthier, P., Cardinali, C., Langland, R., Tsyrulnikov, M. and co-authors. 2008. An update on THORPEX-related research in data assimilation and observing strategies. *Nonlin. Processes Geophys.* **15**, 81–94.
- Reynolds, C. A., Peng, M. S., Majumdar, S. J., Aberson, S. D., Bishop, C. H. and co-authors. 2007. Interpretation of adaptive observing guidance for Atlantic tropical cyclones. *Mon. Wea. Rev.* **135**, 4006–4029.

- Skamarock, W. C., Klemp, J. B., Dudhia, J., Gill, D. O., Barker, D. M. and co-authors. 2005. A description of the Advanced Research WRF version 2. NCAR Tech. Note NCAR/TN-468 + STR, 88 pp.
- Snyder, C. and Zhang, F. 2003. Assimilation of simulated Doppler radar observations with an ensemble Kalman filter. *Mon. Wea. Rev.* **131**, 1663–1677.
- Szunyogh, I., Kostelich, E. J., Gyarmati, G., Kalnay, E., Hunt, B. R. and co-authors. 2008. A local ensemble transform Kalman filter data assimilation for the NCEP global model. *Tellus* **60**, 113–130.
- Thompson, G., Rasmussen, R. M. and Manning, K. 2004. Explicit forecasts of winter precipitation using an improved bulk microphysics scheme. Part I: description and sensitivity analysis. *Mon. Wea. Rev.* **132**, 519–542.
- Tippett, M. K., Anderson, J. L., Bishop, C. H., Hamill, T. M. and Whitaker, J. S. 2003. Ensemble square root filters. *Mon. Wea. Rev.* **131**, 1485–1490.
- Torn, R. D. 2010. Performance of a mesoscale ensemble Kalman filter (EnKF) during the NOAA high-resolution hurricane test. *Mon. Wea. Rev.* **138**, 4375–4392.
- Torn, R. D. and Hakim, G. J. 2008. Performance characteristics of a pseudo-operational ensemble Kalman filter. *Mon. Wea. Rev.* **136**, 3947–3963.
- Torn, R. D. and Hakim, G. J. 2009. Ensemble data assimilation applied to RAINEX observations of Hurricane Katrina (2005). *Mon. Wea. Rev.* **137**, 2817–2829.
- Torn, R. D., Hakim, G. J. and Snyder, C. 2006. Boundary conditions for limited-area ensemble Kalman filters. *Mon. Wea. Rev.* **134**, 2490–2502.
- Velden, C., Daniels, J., Stettner, D., Santek, D., Key, J. and co-authors. 2005. Recent innovations in deriving tropospheric winds from meteorological satellites. *Bull. Am. Meteorol. Soc.* **86**, 205–223.
- Weissmann M., Harnisch, F., Wu, C.-C., Lin, P.-H., Ohta, Y. and co-authors. 2011. The influence of dropsondes on typhoon track and mid-latitude forecasts. *Mon. Wea. Rev.* **139**, 908–920.
- Weng, Y., Zhang, M. and Zhang, F. 2011. Advanced data assimilation for cloud-resolving hurricane initialization and prediction. *Computing in Science and Engineering* **13**, 40–49.
- Whitaker, J. S. and Hamill, T. M. 2002. Ensemble data assimilation without perturbed observations. *Mon. Wea. Rev.* **103**, 1913–1924.
- Whitaker, J. S., Hamill, T. M., Wei, X., Song, Y. and Toth, Z. 2008. Ensemble data assimilation with the NCEP Global Forecast System. *Mon. Wea. Rev.* **136**, 463–482.
- Wu, C.-C., Chen, J.-H., Majumdar, S. J., Peng, M. S., Reynolds, C. A. and co-authors. 2009. Inter-comparison of targeted observation guidance for tropical cyclones in the Northwestern Pacific. *Mon. Wea. Rev.* **137**, 2471–2492.
- Wu, C.-C., Chou, K.-H., Lin, P.-H., Aberson, S. D., Peng, M. S. and co-authors. 2007. The impact of dropwindsonde data on typhoon track forecasts in DOTSTAR. *Wea. Forecast.* **22**, 1157–1176.
- Wu, C.-C., Chou, K.-H., Wang, Y. and Kuo, Y.-H. 2006. Tropical cyclone initialization and prediction based on four-dimensional variational data assimilation. *J. Atmos. Sci.* **63**, 2383–2395.
- Wu, C.-C., Lien, G.-Y., Chen, J.-H. and Zhang, F. 2010. Assimilation of tropical cyclone track and structure based on the ensemble Kalman filter (EnKF). *J. Atmos. Sci.* **67**, 3806–3822.
- Wu, C.-C., Lin, P.-H., Aberson, S., Yeh, T.-C., Huang, W.-P. and co-authors. 2005. Dropwindsonde Observations for Typhoon Surveillance near the Taiwan Region (DOTSTAR): an overview. *Bull. Am. Meteorol. Soc.* **86**, 787–790.
- Xiao, Q., Chen, L. and Zhang, X. 2008. Evaluations of BDA scheme using the advanced research WRF (ARW) model. *J. Appl. Meteorol. Climatol.* **48**, 680–689.
- Xiao, Q., Kuo, Y.-H., Zhang, Y., Barker, D. M. and Won, D.-J. 2006. A tropical cyclone bogus data assimilation scheme in the MM5 3D-Var system and numerical experiments with Typhoon Rusa (2002) near landfall. *J. Meteorol. Soc. Japan* **84**, 671–689.
- Xiao, Q., Zou, X. and Wang, B. 2000. Initialization and simulation of a landfalling hurricane using a variational bogus data assimilation scheme. *Mon. Wea. Rev.* **129**, 2252–2269.
- Xue, M. and Martin, W. J. 2006. A high-resolution modeling study of the 24 May 2002 case during IHOP. Part I: numerical simulation and general evolution of the dryline and convection. *Mon. Wea. Rev.* **134**, 149–171.
- Yamaguchi, M., Iriguchi, T., Nakazawa, T. and Wu, C.-C. 2009. An observing system experiment for Typhoon Conson (2004) using a singular vector method and DOTSTAR data. *Mon. Wea. Rev.* **137**, 2801–2816.
- Zhang, F. 2005. Dynamics and structure of mesoscale error covariance of a winter cyclone estimated through short-range ensemble forecasts. *Mon. Wea. Rev.* **133**, 2876–2893.
- Zhang, F., Meng, Z. and Aksoy, A. 2006. Test of an ensemble Kalman filter for mesoscale and regional-scale data assimilation. Part I: perfect model experiments. *Mon. Wea. Rev.* **134**, 722–736.
- Zhang, F., Snyder, C. and Sun, J. 2004. Impacts of initial estimate and observation availability on convective-scale data assimilation with an ensemble Kalman filter. *Mon. Wea. Rev.* **132**, 1238–1253.
- Zhang, F., Weng, Y., Sippel, J. A., Meng, Z. and Bishop, C. H. 2009. Cloud-resolving hurricane initialization and prediction through assimilation of Doppler radar observations with an ensemble Kalman filter. *Mon. Wea. Rev.* **137**, 2105–2125.
- Zhu, Y., Iyengar, G., Toth, Z., Tracton, M. S. and Marchok, T. 1996. Objective evaluation of the NCEP global ensemble forecasting system. Preprints, In: *Proceedings of the 15th Conference on Weather Analysis and Forecasting*. Norfolk, VA, AMS, J79–J82.
- Zou, X. and Xiao, Q. 2000. Studies on the initialization and simulation of a mature hurricane using a variational bogus data assimilation scheme. *J. Atmos. Sci.* **57**, 836–860.